TISSUE ENGINEERING: Part A
Volume 21, Numbers 7 and 8, 2015

DOI: 10.1089/ten.tea.2014.0535

Differential Effects of Culture Senescence and Mechanical Stimulation on the Proliferation and Leiomyogenic Differentiation of MSC from Different Sources: Implications for Engineering Vascular Grafts

Maxwell T. Koobatian, MS,[1] Mao-Shih Liang, PhD,[2] Daniel D. Swartz, PhD,[1,3,4] and Stelios T. Andreadis, PhD[2,4,5]

We examined the effects of senescence on the proliferation and leiomyogenic differentiation potential of mesenchymal stem cells (MSCs) isolated from bone marrow (BM-MSCs) or hair follicles (HF-MSCs). To this end, we compared ovine HF-MSCs and BM-MSCs in terms of their proliferation and differentiation potential to the smooth muscle cell lineage. We discovered that HF-MSCs are less susceptible to culture senescence compared with BM-MSCs. We hypothesized that application of mechanical forces may enhance the contractility and mechanical properties of vascular constructs prepared from senescent MSCs. Interestingly, HF-MSCs and BM-MSCs responded differently to changes in the mechanical microenvironment, suggesting that despite phenotypic similarities, MSCs from different anatomic locations may activate different pathways in response to the same microenvironmental factors. In turn, this may also suggest that cell-based tissue regeneration approaches may need to be tailored to the stem cell origin, donor age, and culture time for optimal results.

Introduction

Adult stem cells such as mesenchymal stem cells (MSCs) show significant proliferation and differentiation potential, thereby presenting a promising cell source for tissue regeneration. MSCs have been widely investigated for clinical use in over 200 clinical trials to treat a variety of degenerative diseases, including neurological disorders, inflammation, brain and spinal cord injury, kidney, skin, or cardiac diseases.[1–3] Clinical trials require large quantities of high-quality MSCs reaching up to 10^{10} cells per treatment.[4] However, several studies have shown that the proliferation and differentiation potential of the MSC depends heavily on donor age.[5–9] In addition, culture senescence limits MSC culture time to about 8–10 passages, thereby preventing their expandability to the large cell numbers required for cellular therapies.[6,10,11] This is a major concern, as the patients mostly in need for cellular therapies in general and for vascular grafts in particular are elderly.

The mechanical microenvironment has been shown to play an important role in stem cell differentiation. For cells in culture, the mechanical properties, for example, stiffness and porosity, of the underlying substrate have been implicated in stem cell self-renewal and differentiation.[12–18] In addition, application of physiological forces, such as shear stress, pulsatile pressure, or cyclic stretching, have been shown to influence extracellular matrix (ECM) synthesis and the mechanical properties of 3D tissue constructs.[19–24] These studies prompted us to hypothesize that application of mechanical forces might act synergistically with soluble signals to improve differentiation of the senescent MSC into mature contractile smooth muscle cell (SMC).

Previous work from our laboratory showed that the MSC proliferation capacity, leiomyogenic (SMC; in the rest of the text referred to as myogenic) differentiation potential, and the ability of the differentiated cells to generate force were greatly diminished with aging.[8] In the course of our studies, we observed that MSCs from hair follicles (HF-MSCs) exhibited higher proliferation potential compared with those derived from bone marrow (BM-MSCs). These observations prompted us to compare the senescence propensity of HF-MSCs versus BM-MSCs with time in culture. We also

Departments of [1]Physiology and Biophysics, and [2]Chemical and Biological Engineering, University at Buffalo, The State University of New York, Amherst, New York.
[3]Department of Pediatrics, Women and Children's Hospital of Buffalo, University at Buffalo, The State University of New York, Amherst, New York.
[4]Center of Excellence in Bioinformatics and Life Sciences, Buffalo, New York.
[5]Department of Biomedical Engineering, University at Buffalo, The State University of New York, Amherst, New York.

focused on the capacity of HF-MSCs and BM-MSCs to yield functional and contractile SMCs that could be used to regenerate the vascular wall as well as other SMC-containing tissues. In addition, we examined whether application of pulsatile pressure might enhance the contractility and mechanical properties of vascular grafts prepared with senescent HF-MSCs or BM-MSCs. Interestingly, our results showed that MSCs from different anatomic locations exhibited differential response to culture senescence and the mechanical microenvironment.

Materials and Methods

HF-MSC and BM-MSC isolation

HF-MSCs were isolated from skin tissue harvested from two adult sheep under aseptic conditions. Tissue was cut into small pieces and digested with 1 mg/mL collagenase type 1 (Life Technologies, Grand Island, NY) at 37°C for 4 h. Single HFs were then removed from the skin tissue using forceps, filtered through a 40-μm cell filter (BD Biosciences, San Jose, CA), and washed extensively with phosphate-buffered saline (PBS). Individual HFs were then placed in a 96-well cell culture plate (BD Biosciences) and cultured in growth medium (GM). HF-MSCs then migrated onto the cell culture dish and were expanded.[25,26]

BM was aspirated from the femur of three adult sheep under aseptic conditions and plated directly onto six-well cell culture plates precoated with fetal bovine serum (FBS) and cultured in GM. After colonies were observed, cells were then passaged and expanded.

Proliferation assay of BM-MSCs and HF-MSCs

HF-MSCs and BM-MSCs were plated at 3000/cm^2 in triplicates and cultured in GM (Dulbecco's modified Eagle's medium [DMEM] supplemented with 10% MSC-FBS and 1 ng/mL basic fibroblast growth gactor [bFGF]) until they reached 90% confluence. Our previous work has shown the bFGF enhances proliferation and helps maintain the undifferentiated state of adult BM-MSCs.[8] At this point, cells were trypsinized, counted, and replated at the same density. DMEM, FBS, and bFGF were purchased from Life Technologies.

Development of the 24-well pulsation plate

Polycarbonate and stainless steel were used to construct major components (Supplementary Fig. S1a; Supplementary Data are available online at www.liebertpub.com/tea), ensuring the entire 24-well pulsation plate (24-PP) is autoclavable and can be reused. These raw materials were milled using an automated milling machine (HAAS CNC, Oxnard, CA) and designed using FeatureCam software (Salt Lake City, UT). The silastic tubing is distended using air, which enters the 24-PP using a three-way valve and is adjusted using a needle valve (not shown). Air entering the 24-PP is measured in pounds per square inch (PSI). To determine the relationship between PSI and distention, a digital laser micrometer (Keyence, Pasadena, CA) was used to record in real time the distention of the silastic tubing as the PSI was varied from 5 to 25 PSI (Supplementary Fig. S1b). The maximum values from the real-time graphs were then plotted against PSI to determine the distention of the silastic tubing at any desired pressure (Supplementary Fig. S1c).

Preparation of fibrin hydrogel and measurement of compaction

10^6 cells of each cell isolation were suspended in 800 μL of fibrinogen (Enzyme Research Laboratories, South Bend, IN) and mixed with 200 μL of thrombin (Sigma, St. Louis, MO) with final concentrations of 2.5 mg and 2.5 U, respectively. After 1 h, the gels were considered polymerized, released from the plate walls, and allowed to compact over several days in the presence of the compaction medium, which consisted of DMEM, 2% FBS, insulin (2 μg/mL), ε-amino-n-caproic acid (2 mg/mL), L-ascorbic acid (300 μM), and transforming growth factor-β1 (TGF-β1, 2 ng/mL; Biolegend, San Diego, CA). The culture medium was changed daily and gels photographed at indicated time points to calculate the area of each hydrogel.

Preparation of tissue-engineered vessels on the 24-PP

We have extensively reported in the past the preparation of tissue-engineered vessel (TEV) constructs to test for their vasoreactive response to receptor and nonreceptor-mediated pathways.[8,25,27–29] In the current study, the same protocol was used to prepare TEV constructs by polymerizing fibrin hydrogels around the silastic tubing on the 24-PP, which measures 4.75 mm in diameter. 10^6 cells of each cell isolation were suspended in 800 μL of fibrinogen (Enzyme Research Laboratories) and mixed with 200 μL of thrombin (Sigma) with final concentrations of 2.5 mg and 2.5 U, respectively. Gels were considered polymerized after 1 h and released from the plate wall and 24-PP. The vessel medium (VM) consisted of DMEM supplemented with 10% FBS, insulin (2 μg/mL), ε-amino-n-caproic acid (2 mg/mL), L-ascorbic acid phosphate (300 mM), and TGF-β1 (2 ng/mL), and was used to culture all constructs. The medium was changed the following day after gel polymerization, and every other day thereafter. TEV constructs on the 24-PP were kept under static conditions for 1 week, and then pulsed for 1 week periodically (0.3 s/1.7 s distended/rested as reported previously[21,30,31]).

Determining vasoreactivity and mechanical properties for TEVs

After 2 weeks in culture, all TEV constructs were photographed using an EOS 20D Canon camera. Height and thickness of each construct were measured using ImageJ software to determine the cross-sectional area. TEV constructs were then removed from their mandrels and mounted into independent tissue baths submerged in the Krebs–Ringer solution at 37°C using a set of stainless steel hooks linked through the TEV lumen. One set of hooks was connected to a force transducer, while the other was fixed (ADInstruments, Cororado Springs, CO). All tissues were continuously bubbled with 94% oxygen and 6% carbon dioxide to acquire a stable pH of 7.4, a P_{CO2} of 38 mmHg, and a P_{O2} of 500 mHg. The hooks were tightened so that all TEV constructs acquired a basal tension of 1.0 g and were left at equilibrium for at least 30 min. U46619 (1 mM; Sigma), Endothelin-1 (ET-1, 20 nM; Sigma), and potassium chloride (KCl, 118 mM) were added to the tissue baths in sequence after multiple washes between each vasoagonist. Constriction was recorded using a PowerLab data acquisition unit and later analyzed using Chart5 (ADInstruments).

Mechanical properties were measured using the Instron model 3343 with a 5 N load cell (Canton, MA). Tensile stress was delivered at 18 mm/min until TEV constructs broke. Young's Modulus (YM), ultimate tensile strength (UTS), and tensile strain were calculated using Bluehill3 software.

Collagen quantification

The collagen content in TEV constructs was quantified as previously described.[32] TEV constructs were lyophilized and hydrolyzed in 6 N HCl overnight at 110°C. Constructs were then lyophilized a second time and suspended in the assay buffer (5% monohydrate citric acid, 12% trihydrate sodium acetate, 3.4% sodium hydroxide, and 1.2% [v/v] glacial acetic acid, pH at 6.5). After resuspension, debris was removed by centrifugation and 100 μL of supernatant was loaded into a 96-well plate. Fifty microliters of Chloramine-T solution (62 mM; Alfa Aesar, Ward Hill, MA) was added and the solution incubated for 20 min at room temperature (RT). After incubation, 50 μL of Ehrlich's solution (Sigma) was added to each well and incubated at 65°C for ~20 min. Optical Density at 550 nm was measured using a microplate reader (Synergy 4; BioTek, Winooski, VT). Values were compared with a standard curve (0–50 μg/mL of L-hydroxyproline; Sigma). Hydroxyproline values were then converted to collagen concentration using a conversion factor of 7.46 g collagen per gram of hydroxyproline.

Quantitative real-time polymerase chain reaction

RNA was isolated in a 2D culture using an RNeasy kit (Qiagen, Charsworth, CA) and then reverse transcribed using a cDNA synthesis kit (Qiagen). Quantitative real-time polymerase chain reaction (qRT-PCR) was then performed using iCycler (Bio-Rad Laboratories, Hercules, CA). Reaction volumes were 25 μL and contained 1 μL of cDNA, 4uM of each desired primer (Sigma Genosys, Woodlands, TX), and 12.5 μL of 2×IQ TM SYBR Green Supermix (Bio-Rad Laboratories). PCR reactions were carried out for 40 cycles each with a melting point at 95°C for 10 s, annealing at 55°C for 10 s, and an extension at 72°C for 20 s. Fluorescence intensity was recorded at 72°C for 20 s after the extension step of each cycle. Gene expression was calculated using the comparative CT method and normalized to GAPDH. Primer sequences are listed below for *CALD1*, *CNN1*, and *ACTA2*, which encode for SMC proteins Caldesmon, Calponin, and alpha-smooth muscle actin (α-SMA), respectively.

CALD1: 5′-GAAGATGCCGGAAGATGGTT-3′ Forward
5′-TCTTGATGTTGCGGACACCT-3′ Reverse
CNN1: 5′-GTTCCTGCTTCTCCGCGTAT-3′ Forward
5′-ACTGGCATCAGCTGGAGAAC-3′ Reverse
ACTA2: 5′-ATGCTTCTGGCCGCACAACG-3′ Forward
5′-TTCTCGCTCGGCTGTGGTCA-3′ Reverse

The threshold cycle (C_t) of each reaction was defined as the cycle at which the fluorescence was 10 times the mean of standard deviation of the previous 10 cycles, excluding the first one (iCycler software, version 3.0; Bio-Rad Laboratories). Each reaction was performed in triplicates. The relative amount of each cDNA, *R*, was calculated using the average $C_{t,g}$ value for each cDNA and the average $C_{t,GAPDH}$ of the *GAPDH* cDNA as follows:

$$R = 2^{-\Delta C_t}; \qquad \Delta C_t = C_{t,g} - C_{i,GAPDH} \tag{1}$$

Immunostaining

Cells were grown in GM (DMEM supplemented with 10% MSC-FBS and 1 ng/mL bFGF) or VM (DMEM, supplemented with 10% FBS, insulin [2 μg/mL], ε-amino-n-caproic acid [2 mg/mL], L-ascorbic acid [300 mM], and TGF-β1 [2 ng/mL]) for 4 days. Cells were then fixed in 4% paraformaldehyde and permeabilized with 0.1% Triton X-100 in PBS. Cells were then blocked with 5% goat serum in PBS for 1 h and incubated at 4°C with the following antibodies diluted in the blocking buffer: rabbit polyclonal smooth muscle α-actin (α-SMA, 1:200; Abcam; Cambridge, MA), mouse anti-human calponin (1:200; Santa Cruz Biotechnology, Santa Cruz, CA), and rabbit anti-human myosin heavy chain (1:200; Biomedical Technologies, Stoughton, MA). The following day, cells were incubated with Alexa-Fluor 488-conjugated goat anti-mouse or anti-rabbit secondary antibody (1:200; 1 h at RT; Life Technologies), counterstained with Hoechst nuclear dye (1:200 in PBS; 10 min; Sigma), and overlaid with the mounting medium (Electron Microcopy Sciences, Hatfield, PA). Cells that were incubated with only the secondary antibody served as negative controls.

Statistical analysis

All experiments were repeated thrice, each with triplicate samples. Results were analyzed using a two-tailed Student's *t*-test and considered statistically significant if $p < 0.05$.

Results

HF-MSCs exhibited higher proliferation and clonogenic potential than BM-MSCs

We isolated HF-MSCs from two adult ovine donors (HF-1 and HF-2) and BM-MSCs from three adult ovine donors (BM-1, BM-2, BM-3). While the initial doubling times of BM-MSCs were similar (BM-1, -2, -3: 1.38 ± 0.10, 1.46 ± 0.04, 1.41 ± 0.08 days, respectively), the doubling times of BM-MSCs increased significantly with time in culture. After five to six passages, the doubling times of BM-1, -2, and -3 were 6.82 ± 1.81, 5.45 ± 1.40, and 7.63 ± 0.94 days, and the total number of population doublings that BM-1, -2, and -3 underwent in culture were 24.5, 24, and 10.5, respectively. On the other hand, HF-MSCs exhibited higher proliferation rates that were sustained at high levels over time in culture. After 50 days in culture (~10–12 passages), the doubling times for HF-1 increased from 1.07 ± 0.08 to 1.30 ± 0.14 days and for HF-2 from 1.26 ± 0.12 to 1.45 ± 0.10 days (Fig. 1a). The total number of population doublings for HF-1 and -2 was calculated to be 45.5, 24, and 31.5, respectively.

To measure the clonogenic potential, HF-MSCs or BM-MSCs were seeded at low density (10 cells/cm^2) and allowed to grow for 10 days. Cells were then fixed and stained with trypan blue to visualize and count the number of colonies. Only colonies with a diameter larger than 2 mm were counted as those originate from highly proliferative cells, which are more likely to be stem/progenitor cells. All HF-MSC

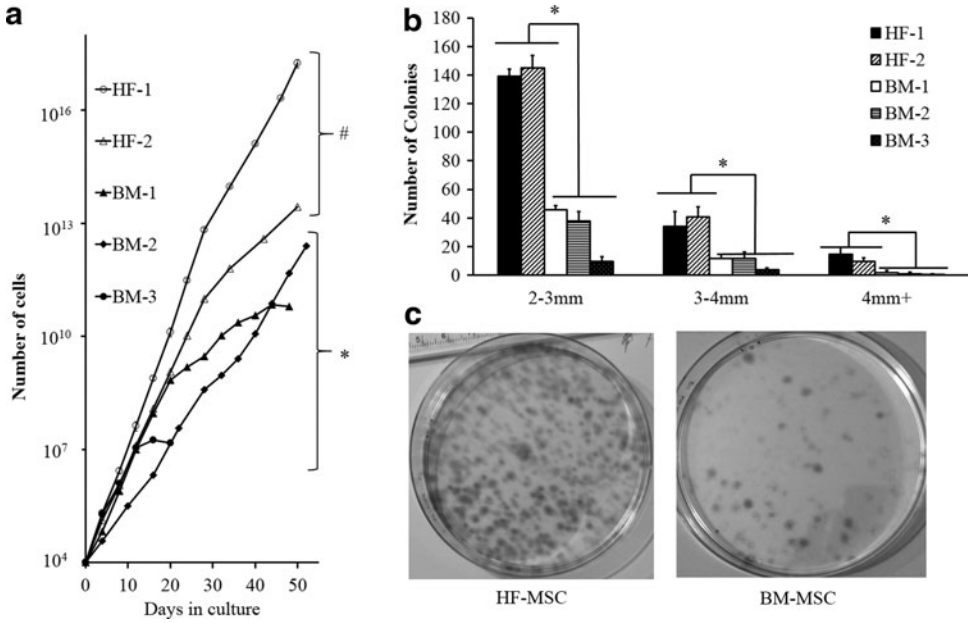

FIG. 1. Proliferation and clonogenic potential of BM-MSCs and HF-MSCs. **(a)** Cells were seeded at 3000 cells per cm^2. Once cells reached near confluence, they were trypsinized and counted at the indicated times. After day 4 and until the conclusion of the experiment, both HF-1 and HF-2 exhibited significantly higher proliferation when compared with all BM cells. The symbols (#) and (*) indicate statistical significance between each HF-MSC and all BM-MSC samples ($p < 0.05$). **(b)** Colony size distribution of HF-MSCs and BM-MSCs. Statistical significance is denoted by *bars* between the indicated samples ($* p < 0.05$). **(c)** HF and BM cells were plated onto 100-mm dishes at 10 cells per cm^2 and cultured for 10 days. Photographs show colonies that originated from single cells. BM, bone marrow; HF, hair follicle; MSC, mesenchymal stem cell.

isolations showed higher clonogenic potential than BM-MSCs (Fig. 1b). The difference between HF-MSCs and BM-MSCs was most profound for colonies between 2 and 3 mm, where HF-1 and HF-2 produced 139 ± 5.2 and 145 ± 8.5 colonies, respectively. By comparison, BM-1, BM-2, and BM-3 yielded only 45.7 ± 3.05, 37.6 ± 6.8, and 9.6 ± 9.6 colonies, respectively. Representative images of HF-1 and BM-1 clones are shown in Figure 1c.

HF-MSCs exhibited significantly lower senescence propensity than BM-MSCs

Next, we compared the two MSC types in terms of cellular senescence by staining for the senescence-associated β-galactosidase (SA-β-Gal) as established previously,[33] using cells between passages 5 and 6. Representative pictures of HF-MSCs and BM-MSCs are shown in (Fig. 2a). Surprisingly, HF-MSCs exhibited minimal levels of senescence, ~1–2% SA-β-gal$^+$ cells, compared with BM-MSCs, which exhibited ~48–58% SA-β-gal$^+$ cells (Fig. 2b).

SMC-specific gene and protein expression in HF-MSCs and BM-MSCs

Next, we examined the differentiation potential of HF-MSCs and BM-MSCs into SMCs. To this end, we measured the levels of several SMC mRNAs using qRT-PCR after culturing cells in myogenic differentiation medium for 3–4 days. Specifically, we measured calponin (*CNN1*), α-SMA (*ACTA2*), and caldesmon (*CALD1*) mRNA as shown in Figure 3. We found that HF-MSCs had nearly equivalent levels of *ACTA2*, *CNN1*, and *CALD1* to BM-1, but significantly higher expression compared with BM-2 and BM-3. In addition, immunostaining for ACTA2, CNN1, and myosin heavy chain (MYH11) showed that under differentiation conditions, both BM-MSCs and HF-MSCs increased expression and induced fibrillar organization of all three proteins, indicating SMC differentiation

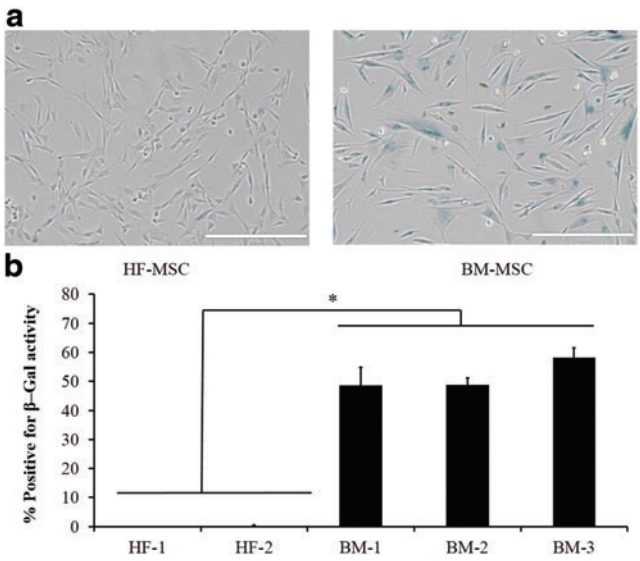

FIG. 2. HF-MSCs displayed significant lower culture senescence propensity than BM-MSCs. **(a)** Representative pictures of BM-MSCs and HF-MSCs stained positive for SA-β-Gal activity. **(b)** Quantification of the percentage of SA-β-gal$^+$ cells from **(a)**. Statistical significance denoted by *bars* between indicated samples ($* p < 0.05$). Color images available online at www.liebertpub.com/tea

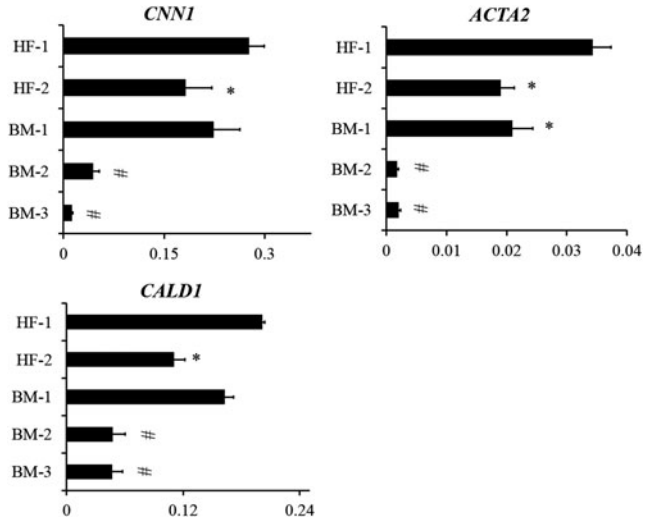

FIG. 3. Expression of SMC-related genes. HF-MSCs and BM-MSCs cultured in the presence TGF-β1 (2 ng/mL) and ascorbic acid (300 μM) for 4 days. Total RNA was isolated, reverse transcribed to cDNA, and used for qRT-PCR to measure the levels of the indicated genes. The data were normalized to GAPDH. Each experiment was done in triplicates. (*) Denotes significance to HF-1 and (#) denotes significance to HF-1, HF-2, and BM-1. qRT-PCR, quantitative real-time PCR; SMC, smooth muscle cell; TGF-β1, transforming growth factor-β1.

(Fig. 4a, b). Interestingly, BM-MSCs appeared bigger and showed more intense filaments, especially of the late SMC protein, MYH11.

HF-MSCs exhibited equivalent or greater vascular contractility than BM-MSCs

Next, we evaluated the ability of HF-MSCs and BM-MSCs to differentiate into functional SMCs and generate force by measuring the following: (i) the compaction of three-dimensional fibrin hydrogels; and (ii) vascular contractility, that is, the isometric tension of fibrin-based tissue constructs in response to vasoreactive agonists.

To this end, cells were embedded in fibrin hydrogels (10^6 cells/mL), and 1 h after polymerization, the gels were released from the plate wall and allowed to compact for 4 days in the presence of the differentiation medium with 2% serum. At the indicated times, the area of each gel was measured using ImageJ and normalized to its initial area (Fig. 5a). Representative images of BM-MSCs and HF-MSCs are shown (Fig. 5b). HF-MSCs exhibited higher compaction when compared with BM-MSCs. Furthermore, HF-1 showed the highest rate of compaction, reaching full compaction after only 30 h. HF-2 exhibited lower compaction rates, but eventually reached similar levels of final compaction as HF-1 (Fig. 5c).

In addition, we measured vascular contractility of constructs prepared with HF-MSCs or BM-MSCs. To this end, we prepared cylindrical tissue equivalents by embedding cells in fibrin hydrogels that were polymerized around 4.75-mm silastic tubing. After being cultured for 2 weeks in differentiation medium, the cells compacted the hydrogels down to ~5% of their original volume, yielding cylindrical constructs with a wall thickness of ~500 μm. At that time, vascular rings were placed in isolated tissue baths to measure isometric tension generated in response to receptor or nonreceptor-mediated vasoagonists.

Interestingly, HF-MSCs displayed very high vascular contractility in response to receptor (ET-1, U46619) or nonreceptor (KCl)-mediated pathways (Fig. 6a, b). HF-2 exhibited significantly higher constriction in the presence of U46619 compared with HF-1 (1280.59 ± 208.54 vs. 786.07 ± 200.57), while HF-1 exhibited significantly greater constriction in the presence of KCl compared with HF-2 (1252.45 ± 216.35 vs. 701.38 ± 192.35). On the other hand, contractility was significantly lower or nonexistent for constructs generated with BM-MSCs. Collectively, our data showed that BM-MSC-based constructs displayed significantly lower contractility compared with HF-MSC constructs.

Differential effects of pulsation on contractility of BM-MSC versus HF-MSC-based vascular constructs

The low contractility of BM-MSCs compared with HF-MSCs, in combination with previous results from our laboratory showing positive effects of pulsatile force on the mechanical properties of vascular constructs,[31] prompted us to hypothesize that mechanical stimulation might enhance contractility, especially of weak contractile BM-MSC-based constructs.

To address this hypothesis, we designed a 24-PP-based device that enables culture of fibrin-based vascular grafts under mechanical stimulation (Supplementary Fig. S1a). Each vascular construct was cultured around a flexible 4.75-mm diameter silastic mandrel, which was pneumatically distended. Four wells were connected to a common compressed air source so that there were six individual channels in the 24-PP. The silastic mandrel distention was determined as a function of pressure using a laser micrometer that measured the mandrel diameter in real time (Supplementary Fig. S1b). Based on these measurements, the tissue constructs were pulsed periodically (0.3 s/1.7 s distended/rested as reported previously[21]) at 0%, 2%, 3.6%, and 5.5% distension for 1 week following 1 week of static culture. At the end of the 2 weeks, the tissues were evaluated for their ability to respond to vasoactive agonists ET-1 (20 nM), U46619 (1 μM), and KCl (118 mM) and compared with static controls.

Interestingly, TEVs containing BM-MSCs responded differently to mechanical stimulation compared with those containing HF-MSCs. Under pulsatile conditions, the vascular contractility of HF-based constructs either remained unaffected (HF-1) or decreased (HF-2) (Fig. 7a–c). Specifically, at 2% distention, vascular contractility of HF-2 constructs decreased significantly in response to U46619 (Fig. 7a) or ET-1 (Fig. 7b) (U46619, static: 1280.6 ± 208.5 Pa vs. pulsed: 473.9 ± 99.9 Pa; ET-1, static: 1373 ± 331.5 Pa vs. pulsed: 602.1 ± 62.1 Pa), but remained unaffected in response to KCl (Fig. 7c).

In contrast, contractility of BM-MSC-based constructs was enhanced by application of pulsatile force (note that BM-3 could not be tested due to difficulties in attaining the large number of cells required for the experiments). Pulsatile force improved the contractility of BM-1 and BM-2-based tissue constructs significantly. Specifically, while

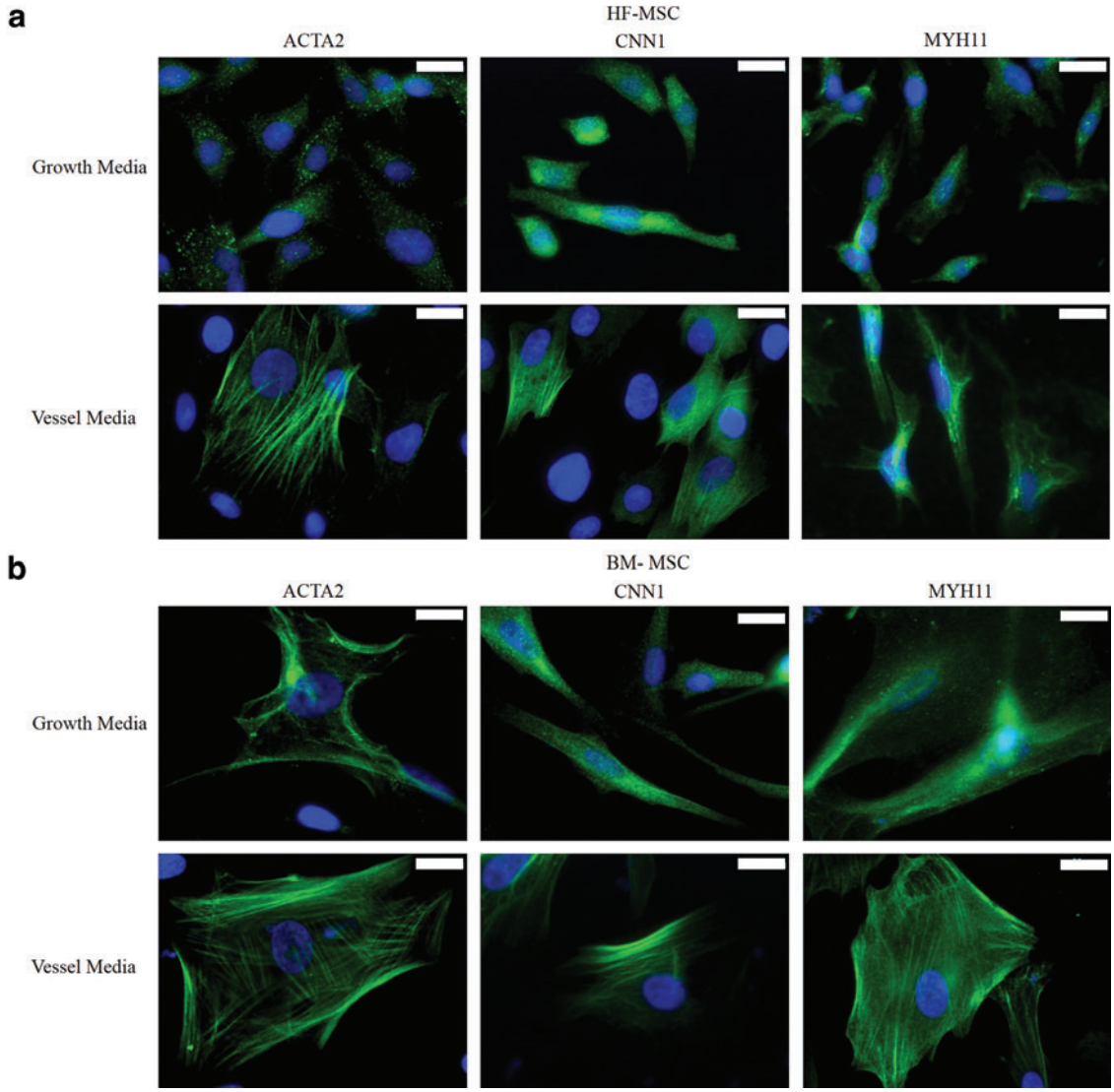

FIG. 4. Expression of SMC-specific proteins. **(a)** HF-MSCs and **(b)** BM-MSCs were seeded at 3000 cells per cm^2 and cultured for 4 days in differentiation or growth medium before immunostaining for smooth muscle-specific proteins α-SMA (ACTA), calponin (CNN1) and myosin heavy chain (MYH11) (*green*). Cell nuclei were counterstained with Hoechst (*blue*). Scale bar: 20 μm. α-SMA, alpha-smooth muscle actin. Color images available online at www.liebertpub.com/tea

BM-1-based TEVs showed no constriction in response to U46619 (Fig. 7d), significant force was measured after pulsation at 2%, 3.6%, or 5.5% distention (84.6 ± 13.5, 331.35 ± 150.2, or 283.1 ± 80.0 Pa, respectively; $p < 0.05$ between static and all pulsed samples, $n = 3$). Similar results were observed in response to ET-1 (Fig. 7e) (static: 220.4 ± 140.2 Pa; pulsed at 2%: 365.1 ± 143; pulsed at 3.6%: 1010.1 ± 123.4 Pa; pulsed at 5.5%: 903 ± 250.4; $p < 0.05$ between static and all pulsed samples, $n = 3$). Interestingly, pulsation had no significant effect on the response to BM-1 TEV constructs to KCl (Fig. 7f). Similar results were observed for BM-2 TEVs, which also improved their response to KCl upon pulsation (static: 45.9 ± 39.8 Pa; pulsed at 2%: 156.75 ± 72.8 Pa; pulsed at 3.6%: 303.8 ± 47.6 Pa; pulsed at 5.5%: 175.5 ± 82.4 Pa; $p < 0.05$ between static and all pulsed samples, $n = 3$) (Fig. 7f).

Differential effects of pulsation on mechanical properties of BM-MSC versus HF-MSC-based vascular constructs

Both HF-MSC and BM-MSC-based grafts exhibited mechanical properties that were strongly dependent on pulsatile force. However, while the mechanical properties of HF-MSC-based constructs decreased, those of BM-MSC-based tissues increased with application of pulsatile force.

HF-1 constructs showed an abrupt reduction in ultimate tensile strength (UTS) and YM at 2% distention, which remained unchanged for a higher force magnitude (UTS, static: 0.75 ± 0.15 MPa; pulsed at 2% distention: 0.23 ± 0.04 MPa; $p < 0.05$, $n = 3$; YM, static: 0.63 ± 0.14 MPa; pulsed at 2% distention: 0.215 ± 0.05; $p < 0.05$, $n = 3$) (Fig. 8a, c). A similar trend was observed for HF-2-based tissues (UTS,

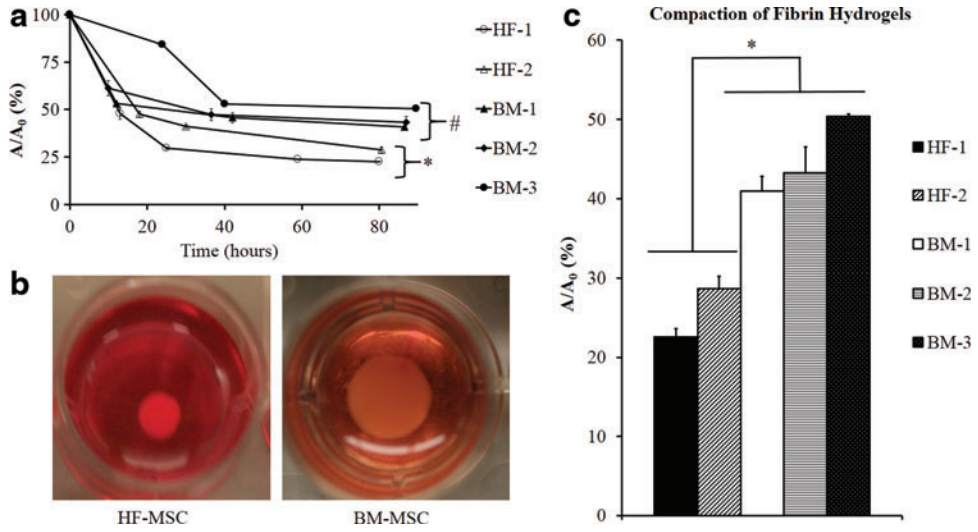

FIG. 5. Hydrogel compaction. HF-MSC and BM-MSC isolations were embedded into fibrin hydrogels and allowed to polymerize in 24-well culture plates forming disks. Gels were detached from the walls of the 24-well plate and allowed to compact over the course of 3–4 days. At indicated times, the gels were photographed and their surface area was calculated using ImageJ software. The ratio of the area of the hydrogel (A) at time, *t*, over the initial area (A_0) was plotted as a function of time. **(a)** Kinetics of fibrin hydrogel compaction for BM-MSCs and HF-MSCs. The symbols (*) and (#) indicate statistical significance between the indicated samples ($p<0.05$). **(b)** Representative pictures of HF-MSC and BM-MSC-containing hydrogels after 80 h of compaction. **(c)** Final hydrogel compaction at $t=80$ h. The *bars* denote statistical significance (* $p<0.05$) between the two groups. The samples within each group are not statistically significant. Color images available online at www.liebertpub.com/tea

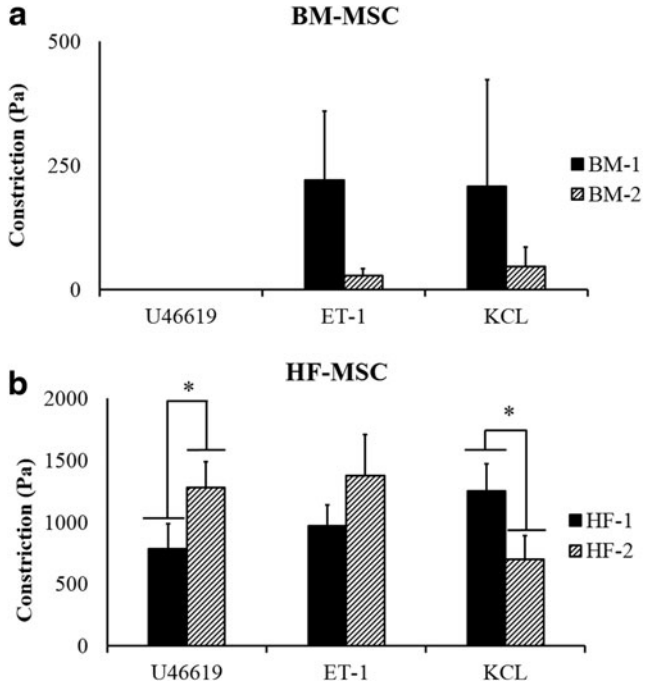

FIG. 6. Vascular contractility of HF-MSC and BM-MSC-based vascular constructs. HF-MSCs and BM-MSCs were embedded in fibrin hydrogels and cultured around mandrels (4.75-mm diameter) for 2 weeks forming cylindrical rings. Vascular contractility (Pa) was measured in the presence of ET-1 (20 nM), U46619 (10^{-6}M), and KCl (118 mM). **(a)** BM-MSC-based TEVs; **(b)** HF-MSC-based TEVs. Statistical significance (* $p<0.05$) is denoted by *bars* between indicated samples. ET-1, Endothelin-1; KCl, potassium chloride; TEV, tissue-engineered vessel.

static: 0.52 ± 0.09; pulsed at 2% distention: 0.27 ± 0.04 MPa; $p<0.05$, $n=3$; YM, static: 0.55 ± 0.14 MPa; pulsed at 2% distention: 0.25 ± 0.07 MPa; $p<0.05$, $n=3$).

On the other hand, BM-MSC constructs exhibited the opposite dependence on pulsatile force. BM-1-based constructs improved significantly upon pulsation (UTS, static: 0.16 ± 0.14; pulsed at 2% distention: 0.25 ± 0.015; pulsed at 3.6%: 0.39 ± 0.076 MPa; pulsed at 5.5%: 0.48 ± 0.09 MPa; YM, static: 0.13 ± 0.11; pulsed at 2% distention: 0.24 ± 0.04 MPa; pulsed at 3.6%: 0.39 ± 0.076 MPa; pulsed at 5.5%: 0.425 ± 0.056 MPa; $p<0.05$, $n=3$) (Fig. 8b, d). Similar results were found for BM-2-based tissues.

Differential effects of pulsatile force on the collagen content of BM-MSC versus HF-MSC-based constructs

Collagen content makes up the majority of ECM content and is generally responsible for the mechanical properties of the vascular wall and other tissues.[34] Since pulsation affected the mechanical properties of HF-MSC and BM-MSC-based tissues, we hypothesized that altered mechanical properties might have been the result of differences in collagen content. Indeed, the collagen content of BM-MSC-based constructs improved significantly as a result of pulsation (Fig. 9a). In contrast, HF-MSC-based tissue constructs exhibited significantly lower collagen content than their BM-MSC counterparts and remained unaffected by application of pulsatile force (Fig. 9b).

Discussion

We report that both the proliferation and myogenic differentiation potential of MSCs from different anatomic locations were affected differently by the time of culture.

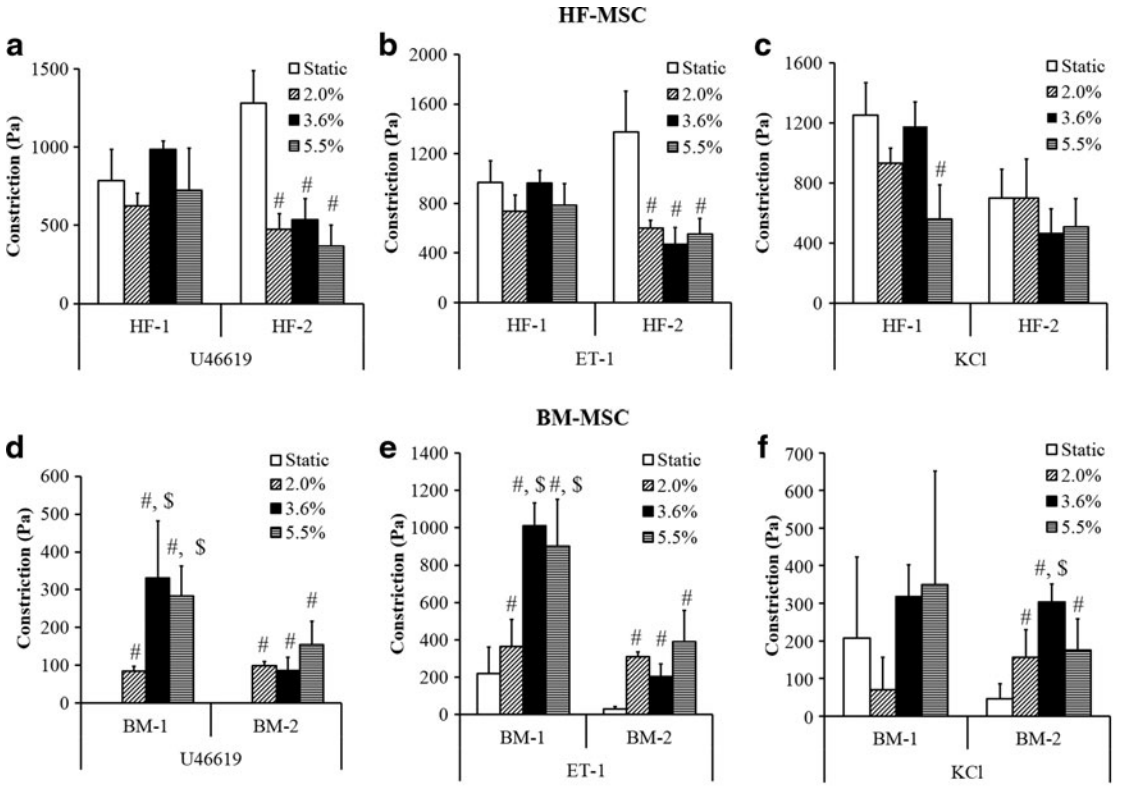

FIG. 7. Effect of pulsation on vascular contractility HF-MSC and BM-MSC-based vascular constructs. HF-MSC and BM-MSC isolations were embedded in fibrin hydrogels and cultured around silastic tubing (4.75-mm diameter) for 2 weeks. Vascular contractility (Pa) was measured in the presence of U46619 (10^{-6}) **(a, d)**, Endothelin-1 (ET-1) (20 nM) **(b, e)** and KCl (118 mM) **(c, f)**. (#) Illustrates significant difference with respect to static samples; ($) denotes significance compared with samples experiencing 2.0% distention ($p < 0.05$).

While BM-MSCs were affected significantly by culture time, HF-MSCs were affected to a much lower extent and could be propagated for many more population doublings. Specifically, BM-MSCs could be propagated up to ~25, while HF-MSCs up to ~45, population doublings. It would be interesting to examine the mechanisms and the pathways at work that explain the delayed senescence exhibited by HF-MSCs compared with BM-MSCs. Such studies may identify potential strategies to delay the onset of senescence in BM-MSCs as well as other adult stem/progenitor cells *in vitro* and perhaps also *in vivo*, thereby increasing the regenerative potential of stem cells.

At the molecular level, we found that mRNA expression of *ACTA2*, *CNN1*, and *CALD1*, as well as the protein level and filamentous organization of α-SMA, CNN1, and MYH11 varied between MSC populations. Previous studies indicated that increased levels of α-SMA correlated with increased contractility for fibroblasts.[35] We reported that neonatal BM-SMCs cultured in the presence of TGF-β1 expressed higher levels of α-SMA and exhibited higher gel compaction and significantly enhanced vascular contractility compared with adult BM-SMCs.[8] Interestingly, HF-1 and HF-2 expressed similar levels of α-SMA, but exhibited far greater hydrogel compaction as well as vascular reactivity in response to receptor and nonreceptor-mediated agonists than BM-MSCs. This suggests that other pathways, perhaps related to actin polymerization and filament organization, might account for the observed functional differences. Notably, all HF-MSCs exhibited far greater contractility than BM-MSCs when differentiated into SMCs, suggesting that either HF-MSCs are able to maintain the activity of contractility-related pathways for longer times in culture or that different molecular effectors may be at work compared with BM-MSCs. Either way, these results are interesting as they indicate that culture time does not affect all MSCs in the body in the same way and points out to the HF-MSC as a highly functional and senescence-resistant cell source for regenerative medicine. In addition, our results point out to the possibility of developing strategies to counteract the effects of cellular senescence based on the molecular understanding of the differences between HF-MSCs versus BM-MSCs.

The differences between BM-MSCs and HF-MSCs with respect to proliferation, culture senescence, and myogenic differentiation prompted us to determine whether these distinct cell populations would behave differently in the presence of the pulsatile force, which mimics the environment of blood vessels *in vivo*. To this end, we prepared fibrin-based cylindrical constructs using either HF-MSCs or BM-MSCs that were pulsed at various degrees of distention. Previous reports have routinely demonstrated that when tissue constructs are subjected to pulsatile forces and strains, mechanical properties, cell alignment, collagen content, as well as vasoconstriction can improve.[30,36–40] Such studies

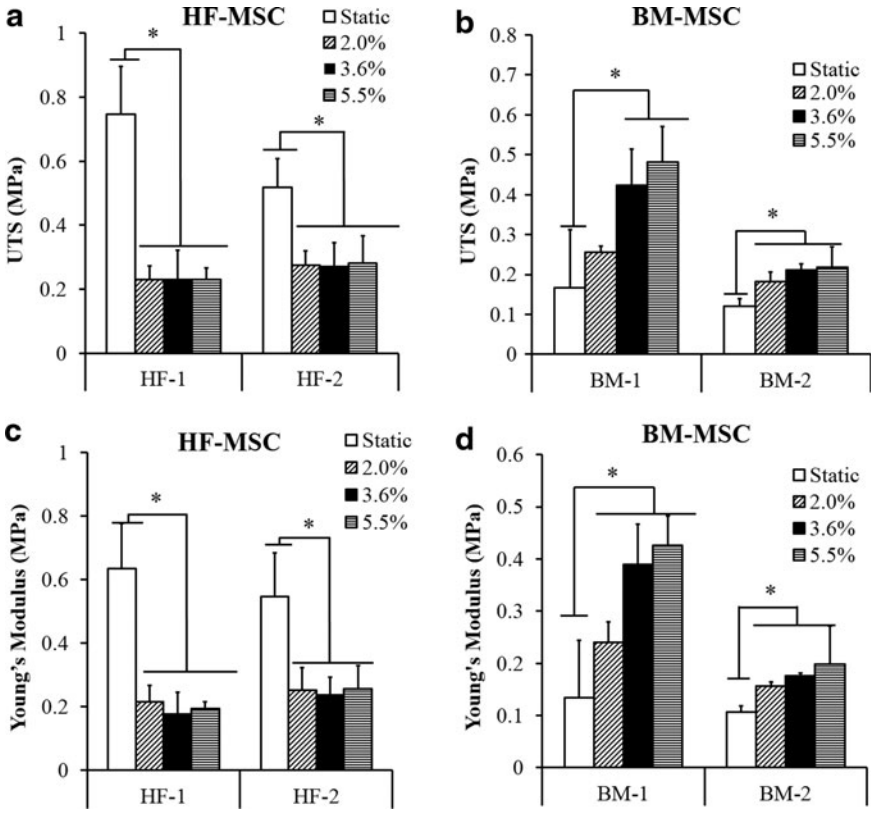

FIG. 8. Effect of pulsation on mechanical properties of HF-MSC and BM TEVs. HF-MSCs or BM-MSCs were embedded in fibrin hydrogels and cultured around silastic tubing (4.75 mm diameter) for 2 weeks. **(a, b)** Ultimate tensile strength (MPa); **(c, d)** Young's Modulus (MPa). Statistical significance ($*p < 0.05$) is denoted by *bars* between the indicated samples.

are in agreement with our current report where BM-MSCs responded favorably when pulsed and vascular contractility improved drastically. Surprisingly, although under static conditions HF-MSC-based TEVs showed much higher constriction than their BM-MSC-based counterparts, their contractility decreased with increasing pulsation. Similar results were obtained for mechanical properties such as UTS, which improved dramatically in BM-MSC-based tissue constructs, but decreased for HF-MSC tissues. These results suggest that the effects of mechanical stimulation of engineered TEVs may depend on the source MSCs that are employed to populate them. They also suggest that while mechanical stimulation may be an effective means to enhance the properties of senescent BM-MSCs and the corresponding tissue constructs, other physical or chemical factors may be better suited for HF-MSCs and perhaps other MSCs as well.

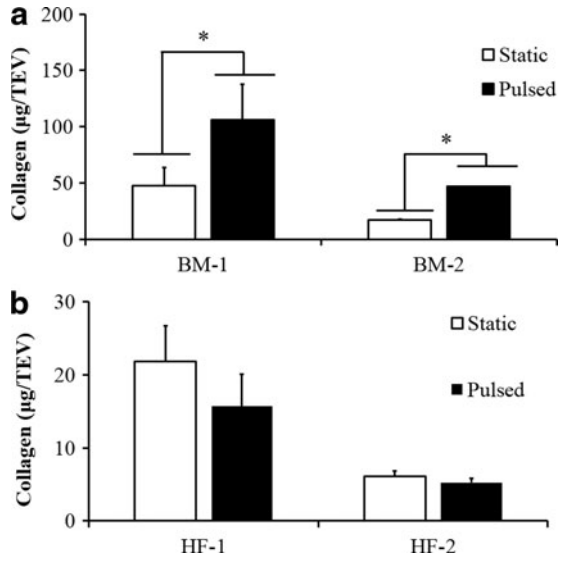

FIG. 9. Effect of pulsation on collagen content. **(b)** HF-MSCs or **(a)** BM-MSCs were embedded in fibrin hydrogels and cultured around silastic tubing (4.75-mm diameter) for 2 weeks. Collagen was measured using the hydroxyproline assay. Statistical significance ($*p < 0.05$) is denoted by *bars* between indicated samples.

Improved vascular reactivity and mechanical properties of BM TEVs under pulsatile conditions correlated with increased collagen content that could be attributed to several mechanisms. Previous work showed that cyclic distention increased collagen expression, which required activation of the Erk1/2 pathway.[30] Other members of the MAP kinase family, such as p46/54 JNK and p38 MAPK, were also activated by cyclic distention. However, in contrast to Erk1/2, activation of p38 negatively regulated procollagen gene expression[41] and in some systems it mediated cell apoptosis in response to mechanical stress. Alternatively, the differences in collagen content could be explained by differential regulation of matrix metalloproteinases (MMPs), which are known to play a major role in the physiological and pathological remodeling of blood vessels.[42–44] Specifically, MMP-2 activity increased when collagen-embedded rat aortic SMCs were subjected to strain, and conversely, MMP inhibition diminished the UTS and YM of tissue constructs.[43] Furthermore, MMP-2 activity was also shown to vary between different cell types, such as human aortic

smooth muscle cells (HASMCs) and human dermal fibroblasts (HDFs), when embedded in collagen hydrogels and subjected to cyclic strain. In contrast to HDFs, prolonged strain increased MMP-2 activity and led to deteriorating mechanical properties of HASMC constructs.[38] These results suggest that MMP activity may be higher in HF-MSCs compared with BM-MSC-based constructs, thereby explaining the differential response to pulsatile pressure. If true, then, better control of matrix degradation might improve the mechanical properties of HF-MSC-based vascular constructs. Understanding the signaling pathways that may be responsible for the observed phenotypic differences between BM-MSCs and HF-MSCs may enable manipulation of their activity through knockdown or inhibition strategies to fine-tune the response of HF-MSCs to mechanical stimulation.

In summary, our study indicates that MSCs isolated from different tissues may exhibit unique phenotypic differences depending on anatomic location. Similarly, phenotypic diversity has been observed with vascular (V)-SMCs *in vivo* between the arterial walls of rats,[45] pigs,[46] and humans.[47] V-SMCs in different locations originate from various developmental lineages, including the neuroectoderm-derived neural crest, lateral plate mesoderm, and paraxial mesoderm, and exhibit phenotypic differences, which have been postulated to affect the propensity of different blood vessels to vascular disease.[48] Consequently, the phenotypic differences of MSCs might also be attributed to their different developmental origin, that is, mesoderm (BM-MSCs) versus neuroectoderm (HF-MSCs). If true, this may suggest that for optimal regenerative potential, the origin of MSCs should be tailored to the developmental origin of the tissue in need of regeneration.

Conclusion

HF-MSCs and BM-MSCs show great promise for regenerative medicine. While BM-MSCs are susceptible to culture senescence, losing their proliferation and differentiation potential within a few passages, HF-MSCs maintain their potential for longer times. In addition, BM-MSC-based tissue constructs exhibit lower contractility and mechanical properties than HF-MSC tissues. In contrast to HF-MSCs, BM-MSC constructs respond positively to mechanical stimulation, exhibiting enhanced ECM synthesis as well as mechanical and contractile properties. Further investigation is required to understand the molecular underpinnings of the differential response of HF-MSCs versus BM-MSCs to culture senescence and mechanical stimulation. The potential effects of such phenotypic differences on the regeneration potential of MSCs is also worthy of investigation.

Acknowledgments

This work was supported by grants from the National Heart and Lung Institute (R01 HL086582) and the New York Stem Cell Foundation (NYSTEM, Contract# C024316) to S.T.A. and D.D.S. The authors thank William Macy, Roger Teagarden, and Gary Olson of the UB Engineering Machine Shop for their help in construction of the 24-PP plate bioreactor. Illustration of the 24-PP was done with the help of Kyle Schlaich.

Disclosure Statement

No competing financial interests exist.

References

1. Alagesan, S., and Griffin, M.D. Autologous and allogeneic mesenchymal stem cells in organ transplantation: what do we know about their safety and efficacy? Curr Opin Organ Transplant **19,** 65, 2014.
2. Griffin, M.D., Elliman, S.J., Cahill, E., English, K., Ceredig, R., and Ritter, T. Concise review: adult mesenchymal stromal cell therapy for inflammatory diseases: how well are we joining the dots? Stem Cells **31,** 2033, 2013.
3. Malgieri, A., Kantzari, E., Patrizi, M.P., and Gambardella, S. Bone marrow and umbilical cord blood human mesenchymal stem cells: state of the art. Int J Clin Exp Med **3,** 248, 2010.
4. Meirelles Lda, S., and Nardi, N.B. Methodology, biology and clinical applications of mesenchymal stem cells. Front Biosci **14,** 4281, 2009.
5. Stenderup, K., Justesen, J., Clausen, C., and Kassem, M. Aging is associated with decreased maximal life span and accelerated senescence of bone marrow stromal cells. Bone **33,** 919, 2003.
6. Baxter, M.A., Wynn, R.F., Jowitt, S.N., Wraith, J.E., Fairbairn, L.J., and Bellantuono, I. Study of telomere length reveals rapid aging of human marrow stromal cells following *in vitro* expansion. Stem Cells **22,** 675, 2004.
7. Hacia, J.G., Lee, C.C., Jimenez, D.F., Karaman, M.W., Ho, V.V., Siegmund, K.D., and Tarantal, A.F. Age-related gene expression profiles of rhesus monkey bone marrow-derived mesenchymal stem cells. J Cell Biochem **103,** 1198, 2008.
8. Han, J., Liu, J.Y., Swartz, D.D., and Andreadis, S.T. Molecular and functional effects of organismal ageing on smooth muscle cells derived from bone marrow mesenchymal stem cells. Cardiovasc Res **87,** 147, 2010.
9. Scruggs, B.A., Semon, J.A., Zhang, X., Zhang, S., Bowles, A.C., Pandey, A.C., Imhof, K.M., Kalueff, A.V., Gimble, J.M., and Bunnell, B.A. Age of the donor reduces the ability of human adipose-derived stem cells to alleviate symptoms in the experimental autoimmune encephalomyelitis mouse model. Stem Cells Transl Med **2,** 797, 2013.
10. Wagner, W., Horn, P., Castoldi, M., Diehlmann, A., Bork, S., Saffrich, R., Benes, V., Blake, J., Pfister, S., Eckstein, V., and Ho, A.D. Replicative senescence of mesenchymal stem cells: a continuous and organized process. PLoS One **3,** e2213, 2008.
11. Bonab, M.M., Alimoghaddam, K., Talebian, F., Ghaffari, S.H., Ghavamzadeh, A., and Nikbin, B. Aging of mesenchymal stem cell *in vitro*. BMC Cell Biol **7,** 14, 2006.
12. McBeath, R., Pirone, D.M., Nelson, C.M., Bhadriraju, K., and Chen, C.S. Cell shape, cytoskeletal tension, and RhoA regulate stem cell lineage commitment. Dev Cell **6,** 483, 2004.
13. Discher, D.E., Janmey, P., and Wang, Y.L. Tissue cells feel and respond to the stiffness of their substrate. Science **310,** 1139, 2005.
14. Engler, A.J., Sen, S., Sweeney, H.L., and Discher, D.E. Matrix elasticity directs stem cell lineage specification. Cell **126,** 677, 2006.
15. Treiser, M.D., Yang, E.H., Gordonov, S., Cohen, D.M., Androulakis, I.P., Kohn, J., Chen, C.S., and Moghe, P.V.

Cytoskeleton-based forecasting of stem cell lineage fates. Proc Natl Acad Sci U S A **107,** 610, 2010.
16. Gao, L., McBeath, R., and Chen, C.S. Stem cell shape regulates a chondrogenic versus myogenic fate through Rac1 and N-cadherin. Stem Cells **28,** 564, 2010.
17. Buxboim, A., and Discher, D.E. Stem cells feel the difference. Nat Methods **7,** 695, 2010.
18. Gilbert, P.M., Havenstrite, K.L., Magnusson, K.E., Sacco, A., Leonardi, N.A., Kraft, P., Nguyen, N.K., Thrun, S., Lutolf, M.P., and Blau, H.M. Substrate elasticity regulates skeletal muscle stem cell self-renewal in culture. Science **329,** 1078, 2010.
19. Niklason, L.E., Gao, J., Abbott, W.M., Hirschi, K.K., Houser, S., Marini, R., and Langer, R. Functional arteries grown *in vitro*. Science **284,** 489, 1999.
20. Kim, B.S., Nikolovski, J., Bonadio, J., and Mooney, D.J. Cyclic mechanical strain regulates the development of engineered smooth muscle tissue. Nat Biotechnol **17,** 979, 1999.
21. Isenberg, B.C., and Tranquillo, R.T. Long-term cyclic distention enhances the mechanical properties of collagen-based media-equivalents. Ann Biomed Eng **31,** 937, 2003.
22. Wang, C., Cen, L., Yin, S., Liu, Q., Liu, W., Cao, Y., and Cui, L. A small diameter elastic blood vessel wall prepared under pulsatile conditions from polyglycolic acid mesh and smooth muscle cells differentiated from adipose-derived stem cells. Biomaterials **31,** 621, 2010.
23. Syedain, Z.H., and Tranquillo, R.T. Controlled cyclic stretch bioreactor for tissue-engineered heart valves. Biomaterials **30,** 4078, 2009.
24. Wang, C., Yin, S., Cen, L., Liu, Q., Liu, W., Cao, Y., and Cui, L. Differentiation of adipose-derived stem cells into contractile smooth muscle cells induced by transforming growth factor-beta1 and bone morphogenetic protein-4. Tissue Eng Part A **16,** 1201, 2010.
25. Liu, J.Y., Peng, H.F., and Andreadis, S.T. Contractile smooth muscle cells derived from hair-follicle stem cells. Cardiovasc Res **79,** 24, 2008.
26. Peng, H.F., Liu, J.Y., Andreadis, S.T., and Swartz, D.D. Hair follicle-derived smooth muscle cells and small intestinal submucosa for engineering mechanically robust and vasoreactive vascular media. Tissue Eng Part A **17,** 981, 2011.
27. Liang, M.S., and Andreadis, S.T. Engineering fibrin-binding TGF-beta1 for sustained signaling and contractile function of MSC based vascular constructs. Biomaterials **32,** 8684, 2011.
28. Liu, J.Y., Peng, H.F., Gopinath, S., Tian, J., and Andreadis, S.T. Derivation of functional smooth muscle cells from multipotent human hair follicle mesenchymal stem cells. Tissue Eng Part A **16,** 2553, 2010.
29. Swartz, D.D., Russell, J.A., and Andreadis, S.T. Engineering of fibrin-based functional and implantable small-diameter blood vessels. Am J Physiol Heart Circ Physiol **288,** H1451, 2005.
30. Syedain, Z.H., Weinberg, J.S., and Tranquillo, R.T. Cyclic distension of fibrin-based tissue constructs: evidence of adaptation during growth of engineered connective tissue. Proc Natl Acad Sci U S A **105,** 6537, 2008.
31. Liang, M.S., Koobatian, M., Lei, P., Swartz, D.D., and Andreadis, S.T. Differential and synergistic effects of mechanical stimulation and growth factor presentation on vascular wall function. Biomaterials **34,** 7281, 2013.
32. Reddy, G.K., and Enwemeka, C.S. A simplified method for the analysis of hydroxyproline in biological tissues. Clin Biochem **29,** 225, 1996.
33. Dimri, G.P., Lee, X., Basile, G., Acosta, M., Scott, G., Roskelley, C., Medrano, E.E., Linskens, M., Rubelj, I., Pereira-Smith, O., *et al.* A biomarker that identifies senescent human cells in culture and in aging skin *in vivo*. Proc Natl Acad Sci U S A **92,** 9363, 1995.
34. Cox, R.H. Passive mechanics and connective tissue composition of canine arteries. Am J Physiol **234,** H533, 1978.
35. Hinz, B., Celetta, G., Tomasek, J.J., Gabbiani, G., and Chaponnier, C. Alpha-smooth muscle actin expression upregulates fibroblast contractile activity. Mol Biol Cell **12,** 2730, 2001.
36. Seliktar, D., Black, R.A., Vito, R.P., and Nerem, R.M. Dynamic mechanical conditioning of collagen-gel blood vessel constructs induces remodeling *in vitro*. Ann Biomed Eng **28,** 351, 2000.
37. Solan, A., Mitchell, S., Moses, M., and Niklason, L. Effect of pulse rate on collagen deposition in the tissue-engineered blood vessel. Tissue Eng **9,** 579, 2003.
38. Seliktar, D., Nerem, R.M., and Galis, Z.S. Mechanical strain-stimulated remodeling of tissue-engineered blood vessel Constructs. Tissue Eng **9,** 657, 2003.
39. Schutte, S.C., Chen, Z., Brockbank, K.G., and Nerem, R.M. Cyclic strain improves strength and function of a collagen-based tissue-engineered vascular media. Tissue Eng Part A **16,** 3149, 2010.
40. Syedain, Z.H., Meier, L.A., Bjork, J.W., Lee, A., and Tranquillo, R.T. Implantable arterial grafts from human fibroblasts and fibrin using a multi-graft pulsed flow-stretch bioreactor with noninvasive strength monitoring. Biomaterials **32,** 714, 2011.
41. Papakrivopoulou, J., Lindahl, G.E., Bishop, J.E., and Laurent, G.J. Differential roles of extracellular signal-regulated kinase 1/2 and p38MAPK in mechanical load-induced procollagen alpha1(I) gene expression in cardiac fibroblasts. Cardiovasc Res **61,** 736, 2004.
42. Meng, X., Mavromatis, K., and Galis, Z.S. Mechanical stretching of human saphenous vein grafts induces expression and activation of matrix-degrading enzymes associated with vascular tissue injury and repair. Exp Mol Pathol **66,** 227, 1999.
43. Seliktar, D., Nerem, R.M., and Galis, Z.S. The role of matrix metalloproteinase-2 in the remodeling of cell-seeded vascular constructs subjected to cyclic strain. Ann Biomed Eng **29,** 923, 2001.
44. Galis, Z.S., and Khatri, J.J. Matrix metalloproteinases in vascular remodeling and atherogenesis: the good, the bad, and the ugly. Circ Res **90,** 251, 2002.
45. Bochaton-Piallat, M.L., Ropraz, P., Gabbiani, F., and Gabbiani, G. Phenotypic heterogeneity of rat arterial smooth muscle cell clones. Implications for the development of experimental intimal thickening. Arterioscler Thromb Vasc Biol **16,** 815, 1996.

46. Hao, H., Ropraz, P., Verin, V., Camenzind, E., Geinoz, A., Pepper, M.S., Gabbiani, G., and Bochaton-Piallat, M.L. Heterogeneity of smooth muscle cell populations cultured from pig coronary artery. Arterioscler Thromb Vasc Biol **22,** 1093, 2002.
47. Li, S., Fan, Y.S., Chow, L.H., Van Den Diepstraten, C., van Der Veer, E., Sims, S.M., and Pickering, J.G. Innate diversity of adult human arterial smooth muscle cells: cloning of distinct subtypes from the internal thoracic artery. Circ Res **89,** 517, 2001.
48. Majesky, M.W. Developmental basis of vascular smooth muscle diversity. Arterioscler Thromb Vasc Biol **27,** 1248, 2007.

Address correspondence to:
Daniel D. Swartz, PhD
Department of Physiology and Biophysics
State University of New York at Buffalo
124 Sherman Hall
3435 Main Street
Buffalo, NY 14214

E-mail: swartzda@buffalo.edu

Stelios T. Andreadis, PhD
Bioengineering Laboratory
Department of Chemical and Biological Engineering
The State University of New York at Buffalo
908 Furnas Hall
Amherst, NY 14260-4200

E-mail: sandread@buffalo.edu

Received: September 8, 2014
Accepted: December 9, 2014
Online Publication Date: February 27, 2015